



OPEN Uniform impact on individual megakaryocytes is essential for efficient *in vitro* platelet production

Andrei K. Garzon Dasgupta^{1,4}, Anaïs Pongérard^{1,4}, Léa Mallo¹, Anita Eckly¹, François Lanza¹, Olivier Boiron², Yannick Knapp³ & Catherine Strassel¹✉

Different approaches are being developed to efficiently produce *in vitro* platelets from cultured megakaryocytes to meet the constant demand of platelet transfusion and serve for research purposes. Recent works have shown that turbulence and periodic stress can significantly enhance platelet yield. Here we have developed and characterized a platelet production device that takes in account these properties. This device is based on the Taylor-Couette reactor in which a suspension is confined and sheared between two concentric cylinders. We have demonstrated that such a system allows obtaining high number of *in vitro* platelets per megakaryocyte with native-like morphology and functional properties. Using the combination of *in silico* and *in vitro* techniques, we claimed that overall turbulent conditions are not sufficient for efficient platelet release, and highlighted the importance of the uniform impact of flow on each megakaryocyte, a property that must be taken into account along with general flow characteristics when designing platelet release bioreactors. In addition, we have demonstrated that our system can be scaled up to large volumes without loss of efficiency, a significant advantage for the industrialization of platelet culture. In conclusion, we have developed a platelet production device with a predictable and highly precise effect on each megakaryocyte.

Keywords Cultured platelets, CFD

Blood platelets are indispensable cell fragments crucial for hemostasis. Following vascular injury, they adhere, become activated, and aggregate to stop the bleeding¹. Dysregulation of platelet count or function, attributed to various disorders or treatments significantly elevates the risk of thrombotic and/or bleeding events²⁻⁴. In such cases, transfusion of platelet concentrates (PCs), sourced from healthy donors, serves as the cornerstone for restoring hemostasis by supplying functional platelets^{5,6}.

The growing significance of *in vitro* platelet production is explained by escalating logistical demands associated with PCs. This stems from demographic shifts towards an aging population, compounded by the limited shelf life of PCs, and the expanding frontier of personalized medicine necessitating immunocompatible platelet transfusions. On an industrial scale, despite the availability of immortalized cell lines facilitating rapid and on demand platelet production⁷, optimizing platelet release efficiency within bioreactors remains a key challenge. Tackling this challenge would not only streamline production methods but would also promise a reduction in production costs.

In vivo platelets are generated by the megakaryocytes (MKs), the largest cells residing in the bone marrow, and their formation results from a unique mechanism within the bloodstream. Once mature, MKs are anchored to sinusoidal vessels, where they extend cytoplasmic extensions called proplatelets. These proplatelets are subsequently released and remodeled by the shear forces inside the circulation culminating in the formation of *bona fide* platelets^{8,9}. Each MK is capable of producing between 800 and 3,000 platelets¹⁰. Platelet release occurs mainly in the sinusoids of the bone marrow and to some extent in the pulmonary microcirculation¹¹. While platelet release *in vivo* is attributed to complex interactions between proplatelets and blood stream still under study^{7,12}, recent results have shown that *in vitro* the most efficient platelet productions can be attributed to high shear stresses, unsteady flows and turbulent flow dynamics^{7,13}. Here, mature cultured MKs in suspension are processed in either batch or continuous mode in systems generating complex flow conditions.

In our pursuit of improving platelet production, we have developed a new platelet producing device capable of creating controlled turbulent flows. Central to our approach is the utilization of a Taylor-Couette (TC)

¹Université de Strasbourg, INSERM, EFS Grand-Est, BPPS UMR-S1255, FMTS, Strasbourg F-67065, France. ²CNRS, Université Aix-Marseille, Ecole Centrale Marseille, IRPHE UMR7342, Marseille F-13000, France. ³Université Avignon, LAPEC EA4278, Avignon F-84000, France. ⁴Andrei K. Garzon Dasgupta and Anaïs Pongérard contributed equally to this work. ✉email: catherine.strassel@efs.sante.fr

model that consists of two concentric cylinders capable of independent rotation (see¹⁴ for review). The use of such a bioreactor was motivated by several compelling factors. Firstly, this system has a well-established characterization and offers a wide range of flow regimes, including laminar, spiral, turbulent featureless and turbulent roll-like^{15,16}. The latter attracted our interest because of the known importance of turbulent conditions in platelet production^{7,13}. Secondly, its design allows for seamless scalability while maintaining the regime and flow parameters, saving valuable development time and resources. This inherent flexibility allows for the maintenance of a desired flow regime across a broad range of volumes, rendering our system highly appealing for platelet release applications in both research and industrial settings.

In this study, we demonstrate that the Taylor-Couette reactor tailored for platelet production yields platelets with morphology and functionality similar to their native counterparts. Furthermore, our computational analysis on a single cell level highlights the importance of uniform impact on individual megakaryocytes within the flow. We show that the system, where flow affects different MK with high variability is less efficient, that the uniform one, despite both having similar overall turbulent conditions.

Results

Taylor-Couette system produces native-like platelets

To address the challenges of large-scale platelet production, our aim was to develop a system capable of facilitating efficient platelet release, adaptable to industrial volume requirements. For this purpose, we opted for a Taylor-Couette system, renowned in fluid mechanics for its ability to generate a diverse range of controllable flow regimes. In such a system, a flow takes place between two coaxial cylinders, each capable of independent rotation, with controllable parameters including the Reynolds number (Re), the cylinder radii ratio (η), the gap width (d), the aspect ratio (height/gap) (I), and the direction and rotational speed of each cylinder^{14,17,18}. In this study, we have self-designed and fabricated a TC system as shown in Fig. 1a, with rotors driven by an external control system enabling independent motor control up to 2,000 RPM. In our setting, we have fixed a gap width (d) of 3 mm, an aspect ratio (I) of 20, cylinder radii ratio (η) of 0.79 and a total system volume (V) of 14.7 mL (Fig. 1a). The dynamic viscosity (μ) of the cultured media is 1.2 cP. For the efficient platelet production we used an operational modality of only inner cylinder rotation (referred as “ICR”) with rotational speed set to 1,500 RPM to reach a differential Reynolds number (Re)¹⁹ of 5,000 and processing time of 30 min. This configuration allowed to produce 79 ± 19 (mean \pm SD, $n = 3$) TC-derived platelets/MK, which is significantly higher ($p = 0.027$) than the platelet yield obtained under static conditions (5 ± 2 plts/MK) (Fig. 1b). We then investigated the quality of TC-derived platelets in terms of morphology, content of granules, expression of several major glycoproteins (GPs) and functionality. Transmission electron microscopy (TEM) analysis revealed that TC-derived platelets exhibited ultrastructural features consistent with donor platelets, including a discoid shape supported by a ring of microtubules and the presence of typical platelet organelles i.e. mitochondria, α and δ granules. The open canalicular system (OCS) was also observed (Fig. 1c). Interestingly, while cultured platelets are classically described as being at least twice as larger as native platelets, TC-derived platelets exhibited a diameter close to that of native platelets (3.4 ± 0.4 μm) (Fig. 1d, Supplementary Fig. S1). Importantly TC-derived platelets still expressed high levels of GPIIb α , GPIX and GPVI (Fig. 1e) without the addition of an ADAM-17 inhibitor (KP-457) to the medium. Shedding of these GPs due to ADAM-17 secretion seems to be significantly lower compared to classical platelet delivery methods, where shedding achieves 50%²⁰. TC-derived platelets were also highly functional as detected by combination of activation-specific antibodies. PAC1 revealed the activated conformation of integrin α IIb β 3 and an anti-P-selectin (P-sel) antibody attested the secretion of alpha granules after activation. In the resting state, platelets showed no activation markers, with only 0.9% of platelets positive for both PAC1 and P-sel. In response to a combination of TRAP and CRP or CRP alone, platelets showed a strong capacity for activation, with 28% and 23% of platelets becoming positive for PAC-1 and P-sel, respectively (Fig. 1f).

TC-derived platelets showed comparable degree of adhesion on fibrinogen (Fg) surface with or without additional stimulation by 1U/mL of thrombin (Thr) (Fig. 1g). 72% TC-derived plts vs. 70% WP (Fg alone) and 83% TC-derived plts vs. 98% WP (Fg + Thr) showed spreading capacity ($n = 3$).

In vivo recirculation of TC-derived platelets in immunodeficient mice was highly efficient after transfusion. Indeed, we have shown a transient increase in platelet count between 15 and 240 min of recirculation followed by their removal similar to native platelets, resulting in an even longer half-life than platelets derived from platelet concentrates (48 h vs. 4 h, TC-derived platelets vs. native, respectively) (Fig. 1h).

Red blood cells do not affect TC-derived platelet production

Red blood cells (RBCs) are abundant in blood vessels. Typically, they concentrate near the center of the vessel, displacing platelets and leukocytes towards the wall, thus creating a RBC-depleted cell free layer (CFL)²¹. However, in microvessels, such as those found in the bone marrow, where the majority of platelets are produced, the CFL decreases, resulting in increased interaction between RBCs and the vessel wall²². This observation prompted us to hypothesize that RBCs could play an active role in platelet formation by colliding with proplatelet extensions and thus facilitate platelet formation. We tested this hypothesis in our system by introducing RBCs at a hematocrit (Ht) of 2%, corresponding to a ratio of 6,000 RBCs to one proplatelet-bearing MK (Fig. 2a). This Ht was carefully selected to avoid altering the system's viscosity and flow conditions²³. Despite the addition of RBCs, the resulting platelet production in our system remained largely unaffected (Fig. 2b), showing that RBCs interaction with proplatelet extensions in our system did not affect overall platelet production.

Turbulent conditions are not sufficient for effective platelet release

Turbulent kinetic energy and shear stress are thought to play significant roles in platelet yield in turbulent systems^{7,13}. However, whether optimal values of these parameters alone are sufficient for effective platelet

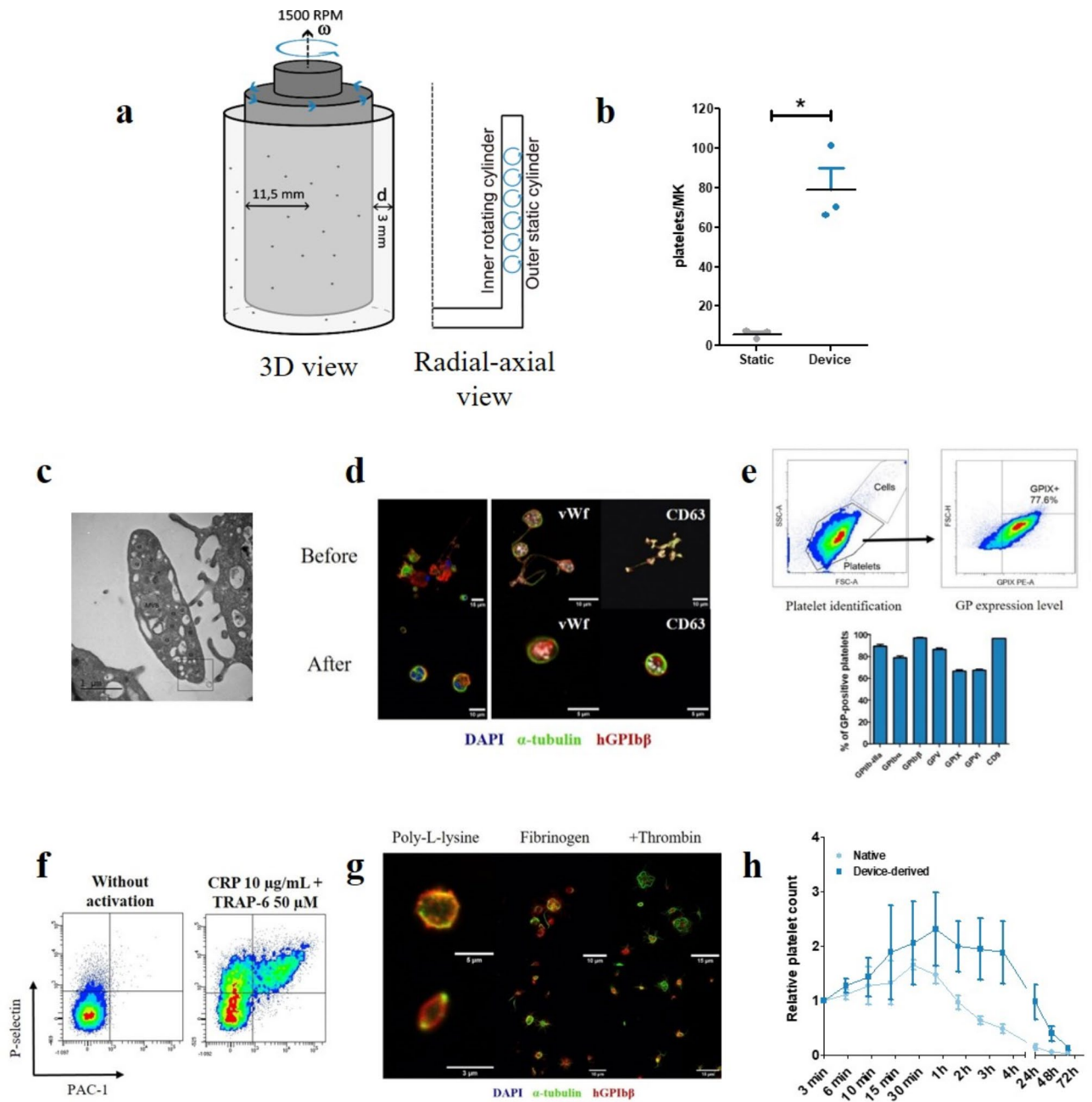


Fig. 1. Characteristics of Taylor-Couette-derived platelets. **a** Scheme of the designed Taylor-Couette (TC) system with only inner cylinder rotation. Radial-axial view depicts roll-like flow behavior. **b** Platelet yields under static conditions and after 30 min processing. **c** Representative transmission electron microscopy image (TEM). **d** Confocal microscopy images of megakaryocytes and platelets before and after liberation by TC system. **e** Glycoprotein expression on the surface of TC-derived platelets. ($n=3$). **f** PAC-1 binding and P-selectin exposure of TC-derived platelets in resting state and after activation by the combination of CRP and TRAP6. **g** Static adhesion of TC-derived platelets on fibrinogen matrix with or without addition of 1U/mL Thrombin. Resting platelets immobilized on poly-L-lysine are shown on the left. **h** Platelet recirculation in a mouse model ($n=3$).

production remains unanswered. For this purpose, we compared two distinct operational modalities: “ICR” and another with inner and outer cylinders in counter rotation with equal angular velocity (referred as “CCR”) (Fig. 2c). Rotational speed in the “CCR” setting was adjusted to have an equal Reynolds number as in the “ICR” setting. Computational fluid dynamics (CFD) showed that general flow parameters, such as turbulent kinetic energy (TKE), Kolmogorov scale (KS) and shear stress (SS) were similarly distributed, as indicated by median values along the volume and interquartile range (IQR) (Table 1).

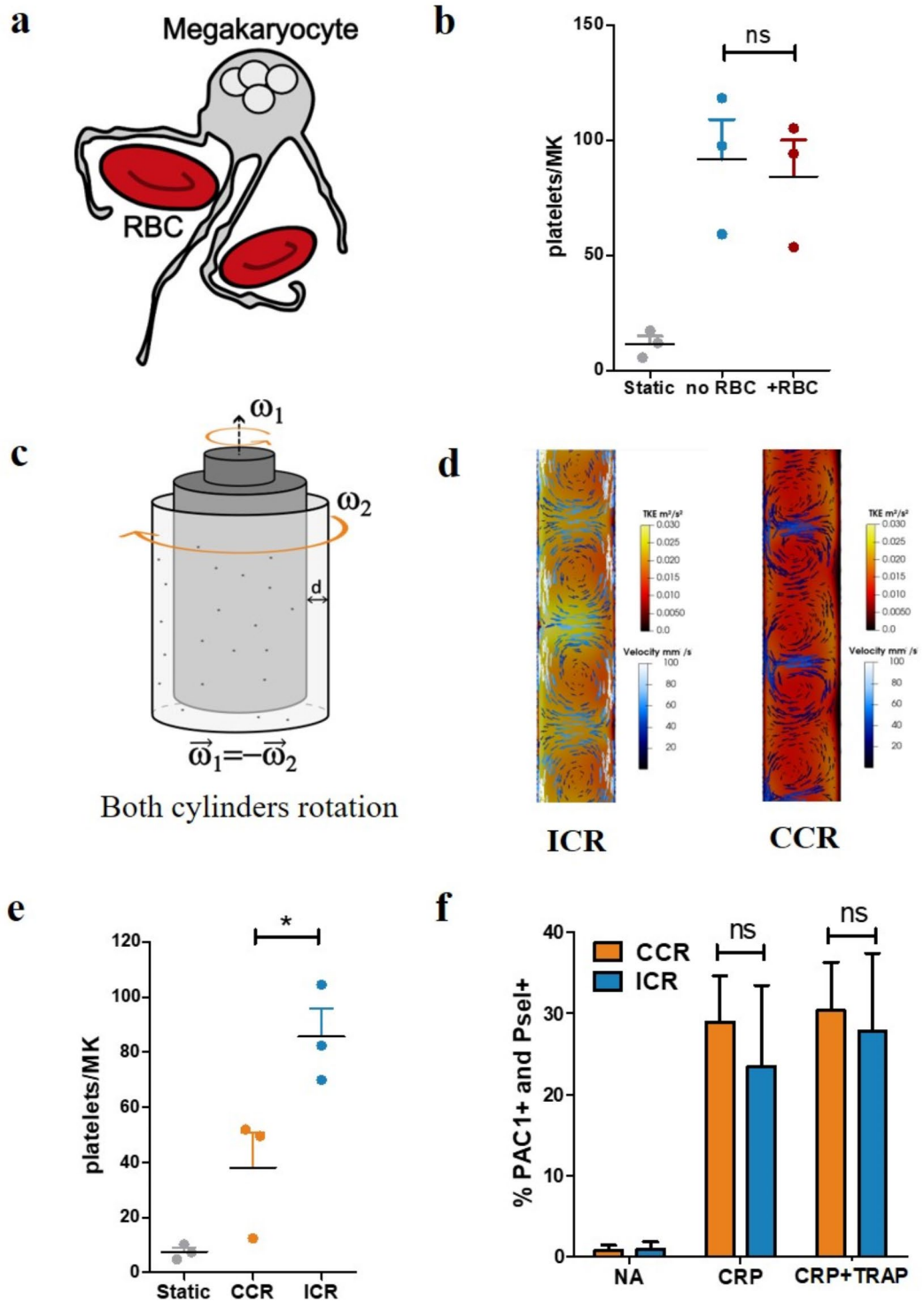


Fig. 2. Platelet production in altered conditions. **a** Scheme of the possible role of red blood cells (RBCs) on platelet liberation. **b** Comparison of platelet yields with or without the presence of RBCs. **c** Scheme of Taylor-Couette system with counter-rotation of inner and outer cylinders (“CCR”). ω – angular velocity. **d** CFD analysis of the Turbulent kinetic energy (TKE) and Velocity fields in the “ICR” and “CCR” systems **e** Comparison of platelet yields obtained in different systems. Paired t-test. $p = 0.0312$ **f** Flow-cytometry evaluation of the activation capacity of platelets derived from the two systems.

NAME	ICR		CCR		Scaled-up ICR	
	IQR	MEDIAN	IQR	MEDIAN	IQR	MEDIAN
General flow parameters						
Reynolds number		5,300		5,300		5,300
Turbulent kinetic energy, m ² /s ²	0.011	0.019	0.012	0.012	0.004	0.016
Kolmogorov scale, μm	13.5	27.5	13.6	35.4	5.5	36.4
Shear stress, Pa	5.3	18.8	6.0	12.7	3.7	15.4
Particle tracking (mean values of 1000 particles)						
Periodic behaviour, % of all	88%		N/A		99%	
Characteristic time, s	0.18		N/A		0.24	
Turbulent kinetic energy, m ² /s ²	0.019		0.002		0.018	

Table 1. Physical parameters for different Taylor-Couette systems IQR-interquartile range, N/A – not applicable.

Although both operational modalities result in flow similarity (identical geometry and Reynolds number) flow patterns are known to differ¹⁶. Notably, our observations revealed contrasting TKE and velocity profiles in the radial-axial plane. In the “ICR” system, a periodic pattern was observed along the height, characterized by alternating high and low values (Fig. 2d, “ICR”). This pattern generated a symmetric velocity profile over the gap that is a unique feature of this modality. Conversely, the “CCR” system exhibited less distinctive behavior (Fig. 2d, “CCR”). This is additionally demonstrated by the λ_2 criterion that is used to identify vortices in the velocity field (Supplementary Fig. S2).

As expected, because of overall turbulent conditions the “CCR” setting improved the platelet yield per MK compared to static condition, but this yield was lower than with the “ICR” modality (Fig. 2e). Furthermore, we observed that platelets released by both modalities exhibited a similar 35-fold increase in activation capacity compared to unstimulated conditions (Fig. 2f). These findings highlight the complex interplay between flow pattern and platelet production, emphasizing the need for a comprehensive understanding of governing parameters when designing platelet release devices.

Increased platelet yield is a consequence of a uniform impact on all cells

To try to elucidate the mechanisms sustaining the increased platelet production in the “ICR” vs. “CCR” operational modalities, we analyzed the behavior of individual MK, by simulating the trajectories of 1,000 randomly placed spheroid particles in the radial-axial plane (Fig. 3a). Interestingly, despite turbulence, the flow structure in the “ICR” modality created recirculation zones, trapping particles in established circular trajectories (Fig. 3b, “ICR”). To estimate the characteristic time associated with this behavior, we calculated the mean time required for a particle to traverse from the near wall region (500 μm) of one cylinder to the near wall region of the other and back. Although this estimation likely underestimates the actual period, it allowed us to compare disturbed trajectories.

For the “ICR”, we observed a mean characteristic time of $T=0.18$ s, with 88% of trajectories exhibiting periodic behavior (Table 1; Fig. 3c). Notably, the characteristic time has a narrow-banded distribution, depicting the uniformity among all the particles. Such behavior directly influenced the impact of the turbulent flow, as indicated by defined mean impact of TKE (Fig. 3c). Interestingly, established circular trajectories lead to periodic impact of TKE at a single particle level over large periods of time (Representative behavior on Fig. 3d, blue graph), which may also contribute to platelet production.

The same particle tracking analysis was performed on the “CCR” modality. In contrast, the trajectories in this modality appeared less coherent with particles less prone to keep trapped in recirculating zones (Fig. 3b, “CCR”, Supplementary Fig. S3). Although our method of calculation of characteristic time was aimed to evaluate the behavior in the “ICR” modality, this approach illustrated disordered behavior in the “CCR”. Here particles exhibit a much broader distribution with a mean characteristic time $T=0.48$ s (Fig. 3c). This may be caused by higher contribution of turbulent fluctuations compared to the mean flow (Fig. 2d). Despite having similar median TKE levels along the geometry (Table 1), real influence of turbulent flow on particles seems to vary drastically (Table 1; Fig. 3c), with only 18% of particles subjected to TKE levels comparable to the “ICR” modality (Fig. 3c, population with $TKE > 0.010$ m²/s²). Impact of TKE on a single particle did not demonstrate periodic behavior (Fig. 3d).

The advantage of the “ICR” modality is that Taylor-Couette system can be easily scaled up by enlarging the radius while maintaining the same flow regime²⁴. A scaled up ($d=3$ mm, $V=30$ mL, $Re=5,300$) TC geometry with “ICR” modality provided a similar platelet yield level as the initial system (Supplementary Fig. S4a). We did not notice changes in particle motion and flow conditions compared to the unscaled system (Table 1, Supplementary Fig. S4b-d), supporting the ability to scale up our device to the desired volumes.

Discussion

In this study, we showed the importance of considering single cell dynamics in the process of designing platelet-release devices and not relying only on general turbulent conditions. The well-defined and predictable impact on each cell in our system allowed us to obtain high platelet yields.

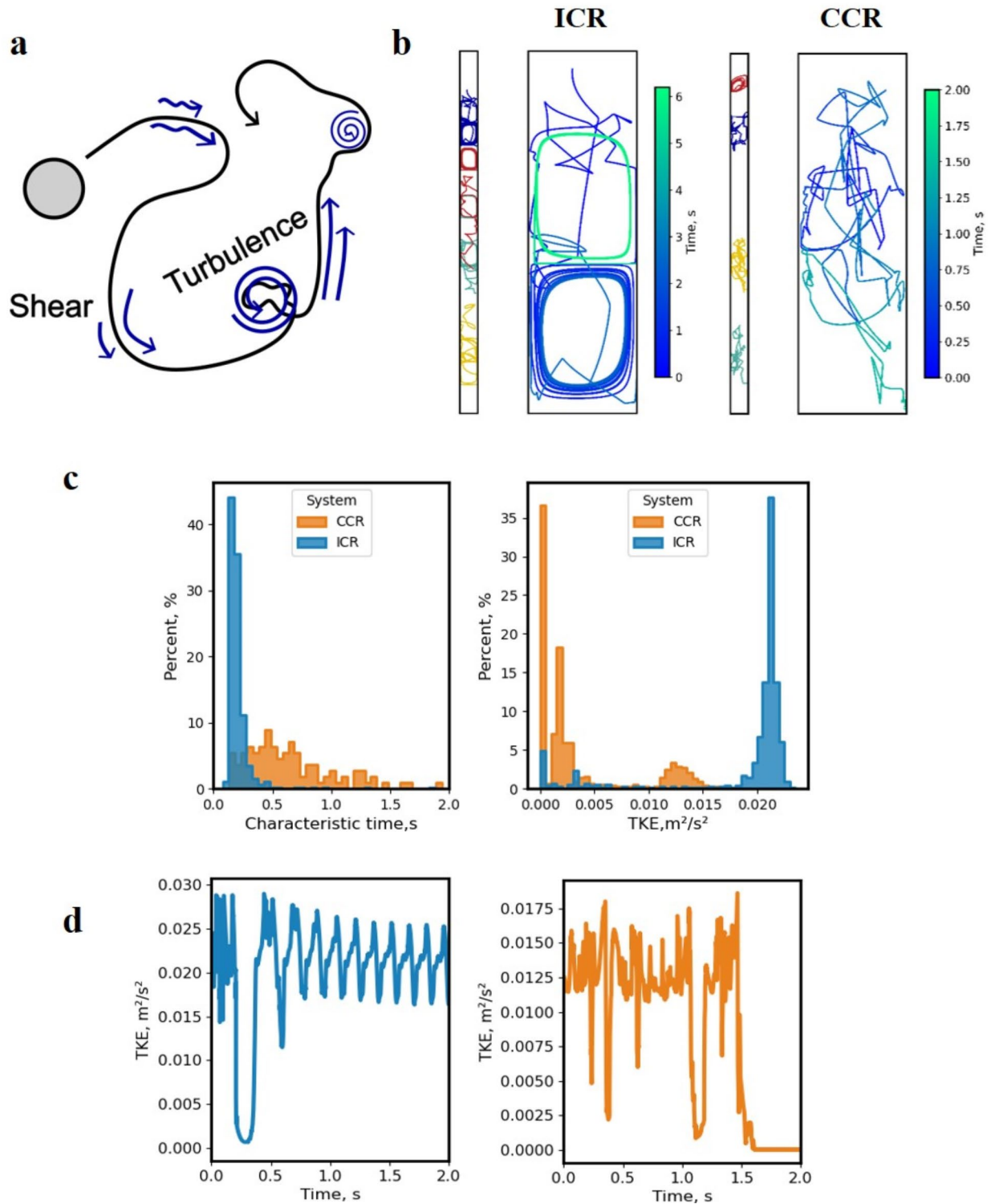


Fig. 3. Particle tracking analysis for “ICR” and “CCR” systems. **a** Scheme of possible impacts on a particle along its trajectory. **b** Representative particle trajectories ($n = 4$) in radial-axial view and close up of one trajectory. **c** Distribution of characteristic time and Turbulent kinetic energy (TKE) values for “CCR” and “ICR” systems. Particles, not showing periodic behavior, were excluded from the “Characteristic time” histogram. **d** The impact of TKE on a single particle along the trajectory for “ICR” (blue) and “CCR” (orange).

Here we introduced a Taylor-Couette-based bioreactor optimized for platelet production that demonstrated good efficiency in producing *bona fide* and functional platelets. Our experimental results showed that platelets produced in this new system retained a native-type morphology, expressed standard levels of glycoproteins and exhibited robust activation capabilities, despite a slight levels of preactivation (<2% PAC-1/P-Sel+) that remains within the norm of other groups^{7,25}. To date, no group has been able to produce platelets in a perfectly inactive state presumably relate to the absence of endothelial cell products such as NO and PGI₂, which are normally present *in vivo* and reduce platelet activation. These platelets showed a prolonged recirculation time in a mouse model, exceeding that of donor-derived platelets. This property has already been well described and has so far been linked to their relatively youthful state, characteristics associated with enhanced circulatory persistence and functionality^{13,26,27}.

Although the slightly pre-activated state of platelets may raise concerns in the context of clinical applications, it is important to note that our group and others^{7,25} have already published results indicating that cultured platelets are capable of limiting blood loss similarly to native platelets. Furthermore, cultured platelets have already been successfully tested in a first-in-human clinical trial²⁸. Collectively, these results suggest that despite a slight pre-activation state, these platelets are fully functional and can be used for transfusion.

In addition to refining device performance, we investigated potential factors affecting platelet production. Specifically, we examined the influence of red blood cells (RBCs) and found that increasing collision rates did not significantly improve platelet release under our experimental conditions. This result might be due to the comparable mass density between RBCs and megakaryocytes (MKs), resulting in MKs behaving similarly to RBCs in our system with low relative velocity between them. Nevertheless, it is crucial to recognize the complex dynamics governing MK-RBC interactions *in vivo*, which cannot be perfectly replicated in our bioreactor setup. Further studies involving both *in vivo* and *in vitro* systems are essential for a full understanding of the role of RBCs in platelet production.

Following our previous study and to optimize the efficiency of platelet production, our system was purposely designed to induce turbulence and periodicity. Intensity of turbulence, represented by Turbulent kinetic energy (TKE), as well as shear stress values were similar to the VerMES system⁷. Interestingly, the size of turbulent vortices, represented by the Kolmogorov scale (27.5–36.4 μm) in all our systems and modalities was similar to the size of MK and lower than the typical length of proplatelet extensions. This matching of characteristic size may also facilitate platelet release, although there is nowadays a controversy on the role played by the Kolmogorov Scale alone²⁹. Another interesting finding was that the chosen modality leads to periodic impact of TKE on a single cell level (Fig. 3d). Our previous study with the “Pipette-mimetic device” (PMD)¹³ showed the importance of periodic loading in the process of *in vitro* platelet production. Despite different nature, VerMES (reciprocal motion), PMD (repeated flow-through system) and our TC bioreactor show periodic behavior, however the typical timescale differ (0.18 s, 0.48 s and 1.2 s, correspondingly). This variety of values shows that although there is an influence of periodicity on platelet production, the topic has still to be studied.

Taking advantage of different possible flow regimes in Taylor-Couette geometry we compared the modality with only inner cylinder rotation “ICR” and two cylinder counter-rotation “CCR”. Although general flow conditions were adjusted to be similar (Table 1), platelet yield in the “CCR” modality appeared to be significantly lower (Fig. 2e). We demonstrated that simply adjusting macroscopic turbulence parameters was not enough to achieve optimal platelet yield and that a detailed analysis of individual cells should now be a major consideration (Fig. 3c, d). We speculate that in both systems platelets are released under similar TKE values. The discrepancy in platelet yield is explained by the fact that in “ICR” the established recirculating zones act as a trap to maintain an optimal turbulent conditions (TKE > 0.10 m²/s²), whereas in “CCR” (Fig. 3c), although vortical structures exist, cells are more prone to escape such structures under the turbulent flow condition. This can lead either to chaotic behavior with similar mean TKE values or to trapping in zones of low turbulence (Fig. 3, Supplementary Fig. S3). As a result, uniform TKE value applied periodically and consistently over a sufficient duration across the entire MK population emerged as an essential determinant of the system’s efficiency. This concept is also observed in the PMD, however there it is achieved by the flow-through nature of the system. The importance of uniform impact was also shown by Okamoto et al.³⁰, illustrating the role of defective turbulent flow space in large-scale platelet production.

Establishing the capability of the Taylor-Couette system for scalable platelet production would require larger quantities of mature MKs, currently only attainable with the use of immortalized MK lines, a step beyond our investigations using MKs derived from peripheral blood CD34+ cells. Nevertheless, our results strongly support that efficient proplatelet production will be attainable with all cell lines, since mechanical interaction, but not the cytokine production, predominantly drives the conversion of megakaryocytic extensions into platelets (see Supplementary Fig. S5). This observation underscores the paramount role of flow in platelet release mechanisms.

Taylor-Couette system has an advantage of straightforward geometrical scalability. In particular, once the width of annular gap is established, scaling-up the system by increasing the height does not drastically perturb the flow conditions, since only the gap size, viscosity and differential rotational speeds play a major role in the device’s behavior. For the chosen “ICR” modality the radius ratio, which is another control parameter for the system, also plays a minor role, allowing scalability of the radius, while maintaining the gap width. We validated this scalability by adjusting the rotation speed to maintain similar Reynolds numbers; ensuring similar flow conditions across different scales (see Supplementary Fig. S4). In order to meet clinical requirements of 300 billion platelets the following configuration of TC reactor can be used for CD34+-derived MK: $R_{int}=1$ m, $d=3$ mm, height (L)= 1 m and rotational speed of 20 RPM. As for the use with another MK cell lines the size of the reactor can be decreased because of the higher initial MK concentration⁷. This geometric scaling approach can be combined with axial flow^{14,31}, as demonstrated in several other application areas. This would create a flow-through system and significantly reduce the operational cost.

Turbulent system with similar impact across all cells

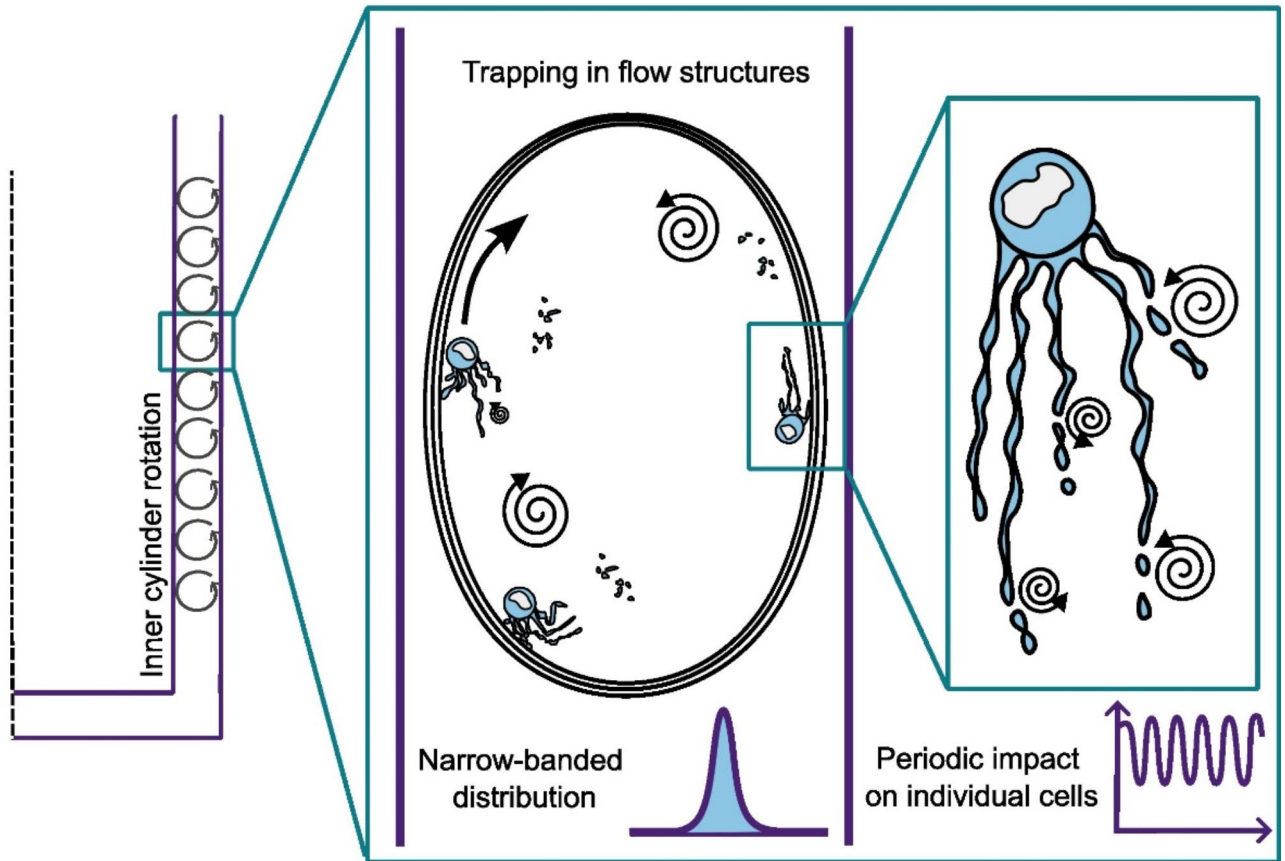


Fig. 4. Platelet release in the Taylor-Couette system at glance. Megakaryocytes get trapped in established recirculation zones with low variability between the cells. The periodic impact from turbulent flow facilitates platelet liberation from proplatelet extensions.

In conclusion, our study has introduced a novel and readily available platelet release system characterized by its high efficiency and scalability, making it easily adaptable to large-scale production. The design of the system ensures the preservation of all established flow properties, including turbulence and, in particular, uniform impact on individual megakaryocytes, a critical parameter that should be considered. Our system allows generation of a predictable and very precise impact on every MK, and on the other hand makes this impact periodic, which may also contribute to platelet production (Fig. 4). This advancement has promising implications for large-scale platelet production by enabling sustained high yields while maintaining process uniformity.

Materials and methods

Taylor-Couette (TC) system description

The Taylor-Couette system comprises two coaxial cylinders capable of independent rotation (Fig. 1a). These cylinders create an annular gap, which was established at a fixed dimension of $d=3$ mm, supported by preliminary investigations. The precise rotational speeds employed are detailed in the section titled “Cultured platelets release.”

Flow simulations in mathematical models

Flow conditions inside the Taylor-Couette system were determined by computational fluid dynamics (CFD) simulations using Fluent 20R2 finite volume software package (ANSYS Inc.). The simulations were performed in 3 consecutive steps. The first one consisted in a simple steady 2D axisymmetric turbulent simulation using a standard k -epsilon model. The boundary conditions were set in terms of linear velocity based on the radius and the angular velocity. During this step, a multizone quad/tri meshing method with inflation was applied to the fluid computational domain resulting in a mesh with $\sim 59,690$ nodes and with the smallest cell size of about 7×10^{-5} m in contact with the walls. Computation was automatically stopped when all residuals had converged to values below 10^{-3} . The results were used to initiate the second step consisting in a steady turbulent flow simulation using Reynolds stress (7 equations) model, which was implemented using the same mesh, boundary

conditions and convergence criteria. The final step consisted in increasing the convergence criteria for the same computation, which automatically ended when all residuals had reached values below 10^{-4} .

The numerical simulations of the flow gave access to pressure and velocity at any position/location of the computational domain and these values were used to define the local gradient of the velocity tensor and other physical quantities of interest.

Particle tracking simulations in mathematical models

To assess the dynamic of MK within the flow, we conducted numerical simulations to track the trajectories of cell-like particles. For this purpose, small inert spherical particles with a diameter of $10\ \mu\text{m}$ were employed to represent the MK. These particles were subjected to flow dynamics using a Lagrangian 2D unsteady model, based on the results obtained from computational fluid dynamics (CFD) simulations. According to the low concentration and size of MK particle-particle and particle-walls were neglected. Only non-reciprocal actions of particles on the flow were considered, leading to the implementation of a one-way coupling approach. A total of 1000 trajectories were computed for particles distributed randomly within the flow domain. Subsequently, the data pertaining to particle histories were subjected to statistical analysis, focusing on the evaluation of particle positions and turbulent kinetic energy distribution throughout the flow domain. The characteristic time was analyzed by calculating the time needed for the particle to go from one near-wall region ($500\ \mu\text{m}$) to another and back. The choice of near-wall region width was made considering the known trajectory paths and switching to $250\ \mu\text{m}$ did not significantly change the results. As each particle can undergo several revolutions throughout the simulation time, the median of this characteristic time was considered for each particle. Particles that during the whole simulation time did not go from one wall to another and back were considered as not having periodic behavior. For the Turbulent kinetic energy, the median value during the simulation time was considered for each particle.

Megakaryocyte differentiation in culture

CD34 + hematopoietic progenitors were extracted from leukodepletion filters (TACSI, Terumo BCT, Zaventem, Belgium) and cultured during 13 days as previously described³².

Cultured platelets release

On day 13 of the experiment platelets were extracted using the Taylor-Couette system for 30 min. $0.5\ \mu\text{M}$ iloprost (Ilomedine $0.1\ \text{mg/mL}$, Bayer AG, Germany) was added just before the liberation to avoid platelet activation by the system. The system used had a geometry characterized by an annular gap of $d = 3\ \text{mm}$ and a total volume of $14.7\ \text{mL}$. The rotational speeds were adjusted to achieve a differential Reynolds number (Re)¹⁹ of 5,000. Specifically, when only the inner cylinder was rotated, the speed was set to 1,500 rpm, while when both cylinders were rotated in opposite directions, each cylinder was set to rotate at 750 rpm.

In upscaled experiments, platelets were collected using a 30 mL Taylor-Couette system with the “ICR” modality and rotational speed 800 rpm to achieve a Reynolds number (Re) of 5,000. The annular gap was consistently maintained at $d = 3\ \text{mm}$. In the static conditions, the medium was collected with 1 mL tips with cut ends to avoid platelet release generated by the pipetting procedure¹³.

Platelet release in the presence of red blood cells

Prior to platelet release utilizing the Taylor-Couette device, red blood cells (RBCs) were added into the system to achieve a final hematocrit of 2%. This specific hematocrit level was selected to ensure that it does not significantly alter the flow viscosity, thereby maintaining flow conditions similar to those without RBCs. In control experiments, RBCs were added after platelet release.

Platelet morphology and ultrastructure

Transmission electron microscopy TC-derived platelets were fixed in 2.5% glutaraldehyde and embedded in Epon. Thin sections were stained with uranyl acetate and lead citrate and examined under a JEol 2100-plus (Jeol, Japan) as previously described²⁶.

Confocal microscopy After fixation in paraformaldehyde, platelets were cytospun, permeabilized with 0.1% Triton X-100 in PBS and incubated sequentially with corresponding antibodies in PBS containing 1% BSA. The cells were then examined under a confocal microscope (TCS SP8, Leica Microsystems, Rueil-Malmaison, France) equipped with an oil objective. Data were acquired with LASAF software, version 1.62 (Leica Microsystems).

In vitro platelet studies

Platelet counting The number of released platelets was estimated in a flow cytometer using tubes containing calibration beads (BD Trucount™, BD Biosciences, San Jose, USA) and antibodies to GPIIb-IIIa (Alexa-488) and GPIba (Alexa-647). The platelet count was expressed as the number of platelets per MK present on day 7 of culture.

Platelet activation Platelets were activated during 10 min at $37\ ^\circ\text{C}$ by the following agonists: collagen-related peptide (CRP) $10\ \mu\text{g/mL}$ or a combination of CRP $10\ \mu\text{g/mL}$ and thrombin receptor-activating peptide-6 (TRAP-6) $50\ \mu\text{M}$. The percentage of activated platelets positive for PAC1 and P-selectin was determined by flow cytometry.

Glycoprotein expression assays The platelet suspension was separated and labeled with antibodies directed against GPIIb-IIIa (Alexa-488), GPIba (Alexa-647), GPIb β (Alexa-568), GPV (Alexa-647), GPIX (Alexa-568)

and CD9. After incubation for 30 min at room temperature, samples were analyzed by flow cytometry. Cytometric analyses were performed using Fortessa X20 (Becton Dickinson, Franklin Lakes, NJ, USA).

Platelet adhesion Following release platelets were washed by sequential centrifugation and resuspended in Tyrode-albumin buffer. Cover glasses were coated with 100 µg/mL fibrinogen for 2 h at room temperature and blocked with 0.1% HSA in phosphate-buffered saline (PBS). Platelets (30 000 platelets/slide) were incubated on the glasses at room temperature for 30 min with or without addition of 1 U/mL of thrombin. Glasses were then washed 3 times with PBS, fixed with 4% 1-paraformaldehyde in PBS for 20 min, washed 3 times with PBS, and labeled with corresponding antibodies. After staining, cover glasses were mounted on glass slides and analyzed under a confocal microscope.

In vivo functionality

Platelets recirculation after transfusion Experiments were performed according to a recent publication²⁶. In brief, following their release, platelets were washed by sequential centrifugation and resuspended in a preservation solution consisting of one-third plasma and two-thirds Intersol (Fresenius Kabi, Homburg, Germany) at a concentration of 5×10^5 platelets/µL. Then, 5×10^7 TC-derived platelets or native human platelets from platelet concentrates transfusion bags were injected through the retro-orbital vein into NSG mice (NOD.Cg-Prkdc scid, Il2rg tm1Wjl/SzJ) previously depleted of macrophages by injection of clodronate liposomes at day -1. Whole blood samples were drawn before and at different time points after transfusion and the proportion of circulating TC-derived platelets or native platelets (NP) recorded in the acquisition gate 3 min after transfusion was arbitrarily set to 1.

Cytokine analysis

Medium obtained before (Control) or after (TC) platelet release was passed through the 0.22 µm filtration membranes. The evaluation of the cytokine levels was performed using Proteome Profiler Human XL Cytokine Array Kit (R&D Systems) according to the manufacturer protocol.

Ethics statement

Human studies were performed according to Helsinki declaration. Control human samples were obtained from volunteer blood donors who gave written informed consent recruited by the blood transfusion center where the research was performed (Etablissement Français du Sang-Grand Est). All procedures were registered and approved by the French Ministry of Higher Education and Research and registered under the number AC_2015_2371. The donors gave their approval in the CODHECO number AC- 2008-562 consent form, in order for the samples to be used for research purposes. NSG mice were housed under pathogen-free conditions and all procedures were performed in accordance with the European Union Guideline 2010/63/EU. The study is reported in accordance to ARRIVE guidelines. The study was approved by the Regional Ethical Committee for Animal Experimentation of Strasbourg, CREMEAS (CEEA 35) and registered under the number 10,669.

Statistical analysis

Results are presented as the mean ± SEM and statistical comparison was performed using paired t-test. (Prism, GraphPad Software Inc., San Diego, CA, USA). *P* values of less than 0.05 were considered to be statistically significant (*P* > 0.05 [ns.]; *P* < 0.05 [*]; *P* < 0.005 [**]).

Data availability

The datasets generated during and/or analysed during the current study are available from the corresponding author on reasonable request.

Received: 15 July 2024; Accepted: 13 November 2024

Published online: 13 January 2025

References

1. Broos, K., Feys, H. B., De Meyer, S. F., Vanhoorelbeke, K. & Deckmyn, H. Platelets at work in primary hemostasis. *Blood Rev.* **25**, 155–167 (2011).
2. Wool, G. D. & Miller, J. L. The impact of COVID-19 disease on platelets and Coagulation. *Pathobiology* **88**, 15–27 (2021).
3. Ma, R., Bi, Y., Kou, J., Zhou, J. & Shi, J. Enhanced procoagulant activity of platelets after chemotherapy in non-small cell lung cancer. *Cancer Biol. Ther.* **18**, 627–634 (2017).
4. Palma-Barqueros, V. et al. Inherited platelet disorders: an updated overview. *IJMS* **22**, 4521 (2021).
5. Strassel, C., Lanza, F. & Gachet, C. Plaquettes sanguines de culture: état de l'art. *Bull. De l'Académie Nationale De Médecine.* **204**, 971–980 (2020).
6. Mookerjee, S., Foster, H. R., Waller, A. K. & Ghevaert, C. J. In vitro-derived platelets: the challenges we will have to face to assess quality and safety. *Platelets* **31**, 724–730 (2020).
7. Ito, Y. et al. Turbulence activates platelet Biogenesis to Enable Clinical Scale Ex vivo production. *Cell* **174**, 636–648e18 (2018).
8. Eckly, A. et al. Megakaryocytes use in vivo podosome-like structures working collectively to penetrate the endothelial barrier of bone marrow sinusoids. *J. Thromb. Haemost.* **18**, 2987–3001 (2020).
9. Thon, J. N. et al. Cytoskeletal mechanics of proplatelet maturation and platelet release. *J. Cell Biol.* **191**, 861–874 (2010).
10. Trowbridge, E. A. et al. The origin of platelet count and volume. *Clin. Phys. Physiol. Meas.* **5**, 145–170 (1984).
11. Lefrançois, E. et al. The lung is a site of platelet biogenesis and a reservoir for haematopoietic progenitors. *Nature* **544**, 105–109 (2017).
12. Bächer, C., Bender, M. & Gekle, S. Flow-accelerated platelet biogenesis is due to an elasto-hydrodynamic instability. *Proc. Natl. Acad. Sci. U.S.A.* **117**, 18969–18976 (2020).
13. Pongérard, A. et al. Development of an efficient, ready to use, blood platelet-release device based on two new flow regime parameters: the periodic hydrodynamic loading and the shear stress accumulation. *New Biotechnol.* **77**, 68–79 (2023).

14. Schrimpf, M. et al. Taylor-Couette reactor: principles, design, and applications. *AIChE J.* **67**, (2021).
15. Andereck, C. D., Liu, S. S. & Swinney, H. L. Flow regimes in a circular couette system with independently rotating cylinders. *J. Fluid Mech.* **164**, 155–183 (1986).
16. Grossmann, S., Lohse, D. & Sun, C. High Reynolds number Taylor-Couette turbulence. *Annu. Rev. Fluid Mech.* **48**, 53–80 (2016).
17. Monico, R. O. et al. Optimal Taylor-Couette flow: Radius ratio dependence. *J. Fluid Mech.* **747**, 1–29 (2014).
18. Mónico, R. O., Stevens, R. J. A. M., Grossmann, S., Verzicco, R. & Lohse, D. Optimal Taylor-Couette flow: direct numerical simulations. *J. Fluid Mech.* **719**, 14–46 (2013).
19. Dubrulle, B. et al. Stability and turbulent transport in Taylor–Couette flow from analysis of experimental data. *Phys. Fluids.* **17**, 095103 (2005).
20. Hirata, S. et al. Selective inhibition of ADAM17 efficiently mediates glycoprotein Iba Retention during Ex vivo generation of Human Induced Pluripotent Stem cell-derived platelets. *Stem Cells Translational Med.* **6**, 720–730 (2017).
21. Kim, S., Ong, P. K., Yalcin, O., Intaglietta, M. & Johnson, P. C. The cell-free layer in microvascular blood flow. *Biorheology* **46**, 181–189 (2009).
22. Li, H., Liu, Z. L., Lu, L., Buffet, P. & Karniadakis, G. E. How the spleen reshapes and retains young and old red blood cells: a computational investigation. *PLoS Comput. Biol.* **17**, e1009516 (2021).
23. Javadi, E., Deng, Y., Karniadakis, G. E. & Jamali, S. In silico biophysics and hemorheology of blood hyperviscosity syndrome. *Biophys. J.* **120**, 2723–2733 (2021).
24. Mónico, R. O., van der Poel, E. P., Verzicco, R., Grossmann, S. & Lohse, D. Exploring the phase diagram of fully turbulent Taylor-Couette flow. *J. Fluid Mech.* **761**, 1–26 (2014).
25. Moreau, T. et al. Large-scale production of megakaryocytes from human pluripotent stem cells by chemically defined forward programming. *Nat. Commun.* **7**, 11208 (2016).
26. Do Sacramento, V. et al. Functional properties of human platelets derived in vitro from CD34+ cells. *Sci. Rep.* **10**, 914 (2020).
27. Allan, H. E. et al. Proteome and functional decline as platelets age in the circulation. *J. Thromb. Haemost.* **19**, 3095–3112 (2021).
28. Chen, S. J., Sugimoto, N. & Eto, K. Ex vivo manufacturing of platelets: beyond the first-in-human clinical trial using autologous iPSC-platelets. *Int. J. Hematol.* **117**, 349–355 (2023).
29. Qi, Y. et al. Fragmentation in turbulence by small eddies. *Nat. Commun.* **13**, 469 (2022).
30. Okamoto, H. et al. Defective flow space limits the scaling up of turbulence bioreactors for platelet generation. *Commun. Eng.* **3**, 77 (2024).
31. Gilchrist, S., Ching, C. Y. & Ewing, D. Heat Transfer Enhancement in Axial Taylor-Couette Flow. in *Heat Transfer: Volume 1 227–233* ASME/EDC, San Francisco, California, USA, doi: (2005). <https://doi.org/10.1115/HT2005-72746>
32. Pongerard, A. et al. Leukodepletion filters-derived CD34+ cells as a cell source to study megakaryocyte differentiation and platelet formation. *JoVE* **62499** <https://doi.org/10.3791/62499> (2021).

Acknowledgements

The authors thank E.Janus-Bell and K.Knez-Hippert for managing animal facility at UMR_S1255. The authors thank E. Bertrand at IRPHE UMR7342 for his help during the development of the TC setup. This work was supported by funds from the Association Nationale de la Recherche et de la Technologie (ANRT to A. Pongerard, PhD candidate).

Author contributions

C.S., AK.GD.,A.P., L.M. O.B., and Y.K conceived and designed the experiments; AK.GD., A.P and L.M. performed the *in vivo* and *in vitro* experiments; A.E. performed electron microscopy; AK.GD., Y.K. and O.B. performed computational fluid dynamics simulations and all associated calculations; AK.GD., A.P, L.M. and C.S analyzed the data; AK.GD., A.P, L.M., F.L., Y.K., O.B., and C.S., discussed the techniques and results; C.S., and Y.K., supervised the work; and AK.GD., A.P, L.M. Y.K., and C.S., wrote the paper.

Declarations

Competing interests

The authors declare no competing interests.

Additional information

Supplementary Information The online version contains supplementary material available at <https://doi.org/10.1038/s41598-024-79949-0>.

Correspondence and requests for materials should be addressed to C.S.

Reprints and permissions information is available at www.nature.com/reprints.

Publisher's note Springer Nature remains neutral with regard to jurisdictional claims in published maps and institutional affiliations.

Open Access This article is licensed under a Creative Commons Attribution-NonCommercial-NoDerivatives 4.0 International License, which permits any non-commercial use, sharing, distribution and reproduction in any medium or format, as long as you give appropriate credit to the original author(s) and the source, provide a link to the Creative Commons licence, and indicate if you modified the licensed material. You do not have permission under this licence to share adapted material derived from this article or parts of it. The images or other third party material in this article are included in the article's Creative Commons licence, unless indicated otherwise in a credit line to the material. If material is not included in the article's Creative Commons licence and your intended use is not permitted by statutory regulation or exceeds the permitted use, you will need to obtain permission directly from the copyright holder. To view a copy of this licence, visit <http://creativecommons.org/licenses/by-nc-nd/4.0/>.

© The Author(s) 2024